Energy 167 (2019) 1224–1235

Contents lists available at ScienceDirect

Energy

journal homepage: www.elsevier.com/locate/energy

Observed and global climate model based changes in wind power potential over the Northern Hemisphere during 1979–2016

Qun Tian [a, b], Gang Huang [a, b, d, e, *], Kaiming Hu [a, c, d], Dev Niyogi [f]

[a] State Key Laboratory of Numerical Modeling for Atmospheric Sciences and Geophysical Fluid Dynamics, Institute of Atmospheric Physics, Chinese Academy of Sciences, Beijing, China
[b] College of Earth Science, University of Chinese Academy of Sciences, Beijing, China
[c] Center for Monsoon System Research, Institute of Atmospheric Physics, Chinese Academy of Sciences, Beijing, China
[d] Joint Center for Global Change Studies, Beijing, China
[e] Laboratory for Regional Oceanography and Numerical Modeling, Qingdao National Laboratory for Marine Science and Technology, Qingdao, China
[f] Department of Agronomy and Department of Earth, Atmospheric, and Planetary Sciences, Purdue University, West Lafayette, IN, USA

ARTICLE INFO

Article history:
Received 6 June 2018
Received in revised form
17 October 2018
Accepted 9 November 2018
Available online 16 November 2018

Keywords:
Wind energy
Wind power potential
Atmospheric stilling
Long-term temporal trend
Cumulative change
CMIP5 model simulation

ABSTRACT

Using an observed dataset, we study the changes of surface wind speeds from 1979 to 2016 over the Northern Hemisphere and their impacts on wind power potential. The results show that surface wind speeds were decreasing in the past four decades over most regions in the Northern Hemisphere, including North America, Europe and Asia. In conjunction with decreasing surface wind speeds, the wind power potential at the typical height of a commercial wind turbine was also declining over the past decades for most regions in the Northern Hemisphere. Approximately 30%, 50% and 80% of the stations lost over 30% of the wind power potential since 1979 in North America, Europe and Asia, respectively. In addition, the evaluation of climate models shows their relatively poor ability to simulate long-term temporal trends of surface winds, indicating the need for enhancing the process that can improve the reliability of climate models for wind energy assessments.

1. Introduction

Renewable energy contributed more than 19% to global final energy consumption in 2015 [1]. In the Paris Agreement, as well as Marrakech Climate Change Conference, renewable energy was a central topic, for it provides a key component of efforts to mitigate climate change [2,3]. Of all renewable energy sources presently used for electricity generation, wind is one of the leaders in terms of installed generating capacity, only exceeded by hydropower [4]. At the end of 2016, the global cumulative wind energy installation was 486.8 GW. In 2016 alone, 54.6 GW was installed worldwide, among which 23.4 GW were installed in China. By the end of 2016, 29 countries had more than 1000 MW installation, including 17 in Europe, five in Asia-Pacific (China, India, Japan, South Korea and Australia), three in North America (Canada, Mexico, the United States), three in Latin America (Brazil, Chile, Uruguay) and one in Africa (South Africa) [3].

Wind energy is generated by air flow through a wind turbine and a process to transform the kinetic energy of the air into electric power. According to the continuity equation of fluid mechanics, the mass flow rate, through a rotor disc of area A, is a function of air density ρ, and air velocity (assumed uniform) U, and is given by [5]:

$$\frac{dm}{dt} = \rho UA \tag{1}$$

The kinetic energy per unit time, or power of the flow is given by:

$$P = \frac{1}{2}\frac{dm}{dt}U^2 = \frac{1}{2}\rho AU^3 \tag{2}$$

The wind power per unit area, or wind power density is:

$$E = \frac{P}{A} = \frac{1}{2}\rho U^3 \tag{3}$$

* Corresponding author. State Key Laboratory of Numerical Modeling for Atmospheric Sciences and Geophysical Fluid Dynamics, Institute of Atmospheric Physics, Chinese Academy of Sciences, Beijing 100080, China.
E-mail address: hg@mail.iap.ac.cn (G. Huang).

https://doi.org/10.1016/j.energy.2018.11.027
0360-5442/

Nomenclature

Abbreviations

AOGCM	Atmosphere-Ocean General Circulation Model
ASOS	Automated Surface Observing System
CMA	Chinese Meteorological Administration
CMDC	China Meteorological Data Service Center
CMIP5	World Climate Research Programme Fifth Coupled. Model Intercomparison Project
ENSO	El Ninõ-Southern Oscillation
ISD	Integrated Surface Database
NAO	North Atlantic Oscillation
NCEI	National Centers for Environmental Information
NOAA	National Oceanic and Atmospheric Administration
PDO	Pacific Decadal Oscillation
PLI	Power law index
QC	Quality Control
RMSD	Root-Mean-Square Difference

Greek symbols

α	Power law index
Γ	Gamma function
κ	Shape parameter in Weibull distribution
ρ	Density of air, kg/m^3

Mathematical symbols

A	Area of a rotor, m^2
c	Scale parameter in Weibull distribution
C	Cumulative change in wind speed, %
D	Root-Mean-Square Difference
E	Wind power density, W/m^2
m	Mass of air, kg
P	Kinetic energy per unit time, W
R	Correlation coefficient
R_g	Regression function of wind speed time series
t	Time, s
U	Wind speed, m/s

It can be assumed that conforms to a probability distribution, for example, two-parameter Weibull distribution [2]:

$$F(U) = 1 - \exp\left[-\left(\frac{U}{c}\right)^{\kappa}\right] \tag{4}$$

The expectation of wind power density can be expressed as:

$$E = \frac{1}{2}\rho c^3 \Gamma\left(1 + \frac{3}{\kappa}\right) \tag{5}$$

Given that wind power density is the cube of wind speed (Equation (3)), a small change in wind speed can have substantial consequences for wind energy resources. In terms of wind electricity output and grid integration, wind speed variability at a short time scale, such as diurnal or synoptic variability, is vital and thus needs to be forecasted. However, when it comes to site selection of wind farms, variability at longer time scales becomes a major concern. While there have been a number of papers on this subject, we focus on long-term temporal trend studies.

Recently, many studies have found that the surface wind speeds were decreasing in recent decades (termed “stilling” [6]). In North America, a change of $-0.05\ ms^{-1}decade^{-1}$ was reported in Canada, while decreases ranging from -0.10 to $-0.19\ ms^{-1}decade^{-1}$ were reported in the United States [7–9]. In Europe, downward trends were also found in many countries, such as Germany ($-0.01\ ms^{-1}decade^{-1}$), the Czech Republic ($-0.08\ ms^{-1}decade^{-1}$), Switzerland ($-0.09\ ms^{-1}decade^{-1}$), France ($-0.05\ ms^{-1}decade^{-1}$) and Greece ($-0.01\ ms^{-1}decade^{-1}$) [10–14]. Similar circumstances occur in Asia, where declines in wind speeds were found in Japan ($-0.03\ ms^{-1}decade^{-1}$), India ($-0.27\ ms^{-1}decade^{-1}$) and P.R. China (ranging from -0.12 to $-0.18\ ms^{-1}decade^{-1}$) [15–19]. In one study covering continental areas in the Northern Hemisphere, a decrease of $5-15\%$ from 1979 to 2008 was reported [20], suggesting that stilling is an increasingly common phenomenon in Europe, North America and Asia. Determining the impact of the stilling on wind energy resources across the Northern Hemisphere is the first question we aim to answer in the current study.

Knowing the changes in the past is not sufficient, a study of how wind energy might evolve over the coming decades becomes necessary. Future climate evolution depends not only on natural variability, but also on anthropogenic forcing. The atmosphere-ocean general circulation model (AOGCM), the primary tool for the investigation of climate system, is currently able to reproduce large-scale natural variability such as El Niño-Southern Oscillation (ENSO) [21]. Although future anthropogenic forcing is hard to predict, possible anthropogenic forcing scenarios were proposed by the World Climate Research Programme Fifth Coupled Model Intercomparison Project (CMIP5), a globally coordinated set of global coupled AOGCMs simulations to project future climate [22]. Simulations of four future scenarios defined by four level of anthropogenic forcing were performed in the CMIP5 and have become the most commonly used dataset for climate projections. In the design of CMIP5, simulations for the historical period are also included, in order to evaluate the performance of models. Chen et al. [23] assessed the performance of several CMIP5 models for reproducing surface wind speeds from 1971 to 2005 over China. Among the nine models chosen for their study, two of them have a large bias to the observations in terms of the annual mean wind speeds, while none exhibits a substantial decline for the historical period. It raises the basic question in wind energy projection: Are CMIP5 simulations of surface wind speeds reliable? This is the second question we aim to answer in this study.

Herein, we analyze changes in surface wind speed by using a carefully quality-controlled dataset consisting of 1038 stations covering the globe (mostly the Northern Hemisphere) for 1979 to 2016. Analysis of surface wind speeds from reanalysis datasets (e.g. NCEP/NCAR, NCEP/DOE, ERA-Interim) is not included in this study, because previous studies suggest that reanalysis datasets are unable to reproduce observed surface wind speed trends [17,20,24]. In addition, we extrapolate surface wind speeds to the typical height of a commercial wind turbine (considered as 80 m) using an empirical algorithm, and examine changes in wind power potential over the past decades. We then conduct a comprehensive evaluation of the simulations for surface wind speeds from 1979 to 2005 from out of the 34 AOGCMs in CMIP5, providing a reference for the reliability of CMIP5 models for wind energy projection.

2. Data and methods

2.1. Data

Observational wind speed time series are available from two sources:

1. The Integrated Surface Database (ISD) [25], initiated by

National Centers for Environmental Information (NCEI), National Oceanic and Atmospheric Administration (NOAA) in 1998, consists of global hourly observations compiled from more than 100 sources. The database includes over 35,000 stations worldwide, of which 14,000 are currently "active" stations updated daily in the database. ISD contains 54 quality control (QC) algorithms which serve to process each of the observations through a series of validity checks, extreme value checks, internal (within the same observation) consistency checks, and external (versus another observation for the same station) consistency checks.

Surface wind speeds from 1979 to 2016 are selected for this study because the number of stations remained stable since late 1970, whereas the spatial coverage of ISD is much less before the early 1970s [25]. To ensure the quality of the wind speed time series, extensive QC processes are conducted and include:

i) Removing stations that were moved from one place to a distant other place, keeping only the stations with less than 0.02° (about 2 km horizontally) and 20 m in elevation relocation, compared to the coordinate of reference time (January 1, 1979, in this case).
ii) Removing records with inhomogeneity, keeping records that passed all the QC checks of ISD and rejecting the others. The remaining hourly records are processed into daily mean data.
iii) Removing stations with large gaps, first, only years with sufficient coverage (more than 360 days) are kept. If one year does not fulfill this requirement, it is removed from the data. Then stations which cover less than 90% of the study period are removed from the list, i.e. stations covering less than 35 years from 1979 to 2016 are excluded.

2. Dataset of Daily Climate Data from Chinese Surface Stations (V3.0) (http://data.cma.cn/data/detail/dataCode/SURF_CLI_CHN_MUL_DAY_V3.0/keywords/v3.0.html), produced by the China Meteorological Data Service Center (CMDC), Chinese Meteorological Administration (CMA), consists of daily values from 824 Chinese surface stations. QC processes of this dataset include extreme value checks, internal consistency checks, external consistency checks and manual verification and correction. The surface wind speed time series for 1979 to 2016 is checked using the extensive QC processes, as is also the case for ISD.

After QC processes, 785 stations remain in NCEI ISD and 351 in the CMDC daily surface observation V3.0. The CMDC dataset is supplementary to NCEI ISD because only 194 Chinese surface stations are openly available for global meteorological data exchange. Consistency check between these two datasets is conducted. The results show that the mean wind speeds for 98 repetitive stations from two sources are consistent, as are the temporal trends. We merge these two datasets into one and name the new dataset the NCEI-CMDC ensemble dataset. The NCEI-CMDC ensemble dataset consists of 1038 stations, including 351 stations from the CMDC dataset and 687 stations from NCEI ISD (98 repetitive stations are excluded).

Surface wind speed simulations are obtained from 34 AOGCMs in CMIP5. Summary of the models used in this work is listed in Table 2. Monthly values from historical runs with both natural and anthropogenic forcing are used in the analyses. It is worthy to note that surface wind speeds derived from CSIRO-MK3.6 are for a nominal height of 2 m, while surface wind speeds from all other AOGCMs are outputted at 10 m. In order to compare with observations, we interpolated the monthly model outputs from different spatial resolutions onto the observed sites of the NCEI-CMDC ensemble dataset using bilinear interpolation (i.e., a linear interpolation function on two-dimensional grids [26]).

Table 1
Top 10 cumulative wind power capacity by the end of 2016[a].

Country	MW	%Share
P.R. China	168,732	34.7
USA	82,184	16.9
Germany	50,018	10.3
India	28,700	5.9
Spain	23,074	4.7
UK	14,543	3
France	12,066	2.5
Canada	11,900	2.4
Brazil	10,740	2.2
Italy	9257	1.9
Rest of the world	75,576	15.5
Total top 10	**411,214**	**84**
World total	**486,790**	**100**

[a] Source: Sawyer and Dyrholm, 2017 [3].

2.2. Method

For the trend analysis of the observations and CMIP5 simulations, we compute a first-degree polynomial regression for annual mean wind speeds using the least square method and conduct significance test using *t*-test. The cumulative changes in wind speeds are computed according to the regression functions:

$$C = \frac{Rg(t_{end}) - Rg(t_{start})}{Rg(t_{start})} \tag{6}$$

We adopt this method instead of directly using values of the starting and ending year, because the latter approach would inevitably introduce interannual variabilities into the analysis, and can be regarded as noise in this case.

To examine the issues with respect to wind speeds from relatively low to high values, we compute the percentiles using daily values of each year. The resulting time series are analyzed for trends using first degree polynomial regression and *t*-test to determine whether trends are significant.

In terms of estimating wind power potential, there are typically two approaches according to existing literatures. One directly uses the kinetic energy flux formula (Equation (3)) with observed wind speeds [48,49]. The other employs a wind speed distribution model with parametric fit to the observational data [50–53]. A common model used in the second approach is the two parameter Weibull distribution (see in section 1 (Equation (4) & (5))). The former approach is chosen for this study, because it can provide a straightforward answer on how atmospheric stilling impacts wind energy resources. In order to simplify the discussion, we assume that air density remains constant. Hence, changes in wind power potential are proportional to changes in the cube of wind speeds. The cumulative changes in wind power potential are computed using Equation (6).

Differences in the spatial fields of wind speeds between CMIP5 models and observations in terms of the standard deviation, the correlation coefficient and RMSD are computed. The correlation coefficient is defined by

$$R = \frac{\frac{1}{N}\sum_{n=1}^{N}\left(f_n - \overline{f}\right)\left(r_n - \overline{r}\right)}{\sigma_f \sigma_r} \tag{7}$$

where $\overline{f}$ and $\overline{r}$ are the mean values, and σ_f and σ_r are the standard deviations of spatial fields f and r, respectively. The RMSD is defined by

Table 2
Summary of CMIP5 AOGCMs. Monthly surface wind speeds from 34 AOGCMs are included in this study. Atmospheric resolution of each model is expressed in the form of longitude × latitude grid.

Model name	Institute (country)	Atmospheric resolution	Reference
ACCESS1.0	CSIRO-BOM (Australia)	1.875° × 1.25°	Dix et al., 2013 [27]
ACCESS1.3	CSIRO-BOM (Australia)	1.875° × 1.25°	Dix et al., 2013 [27]
BCC-CSM1.1	BCC-CMA(P.R. China)	2.8° × 2.8°	Xin et al., 2013 [28]
BCC-CSM1.1(m)	BCC-CMA(P.R. China)	160 × 320 T106	Liu et al., 2015 [29]
BNU-ESM	GCESS(P.R. China)	2.8° ×2.8°	Ji et al., 2014 [30]
CanESM2	CCCMA(Canada)	2.8° × 2.8°	Arora et al., 2011 [31]
CMCC-CESM	CMCC(Italy)	3.75° × 3.75°	Fogli et al., 2009 [32]
CMCC-CM	CMCC(Italy)	0.75° × 0.75°	Fogli et al., 2009 [32]
CMCC-CMS	CMCC(Italy)	1.875°×1.875°	Fogli et al., 2009 [32]
CSIRO-Mk3.6.0	CSIRO-QCCCE(Australia)	1.875°×1.875°	Gordon et al., 2010 [33]
FGOALS-s2	LASG-IAP-CAS(P.R. China)	2.81° × 1.66°	Bao et al., 2013 [34]
GFDL-CM3	NOAA GFDL(USA)	1.875°×1.875°	Griffies et al., 2011 [35]
GFDL-ESM2G	NOAA GFDL(USA)	2.5° × 2°	Dunne et al., 2012 [36], Dunne et al., 2013 [37]
GFDL-ESM2M	NOAA GFDL(USA)	2.5°×2°	Dunne et al., 2012 [36], Dunne et al., 2013 [37]
GISS-E2-H	NASA GISS(USA)	2.5° × 2°	Schmidt et al., 2014 [38]
GISS-E2-H-CC	NASA GISS(USA)	1° × 1°	Schmidt et al., 2014 [38]
GISS-E2-R	NASA GISS(USA)	2.5? × 2°	Schmidt et al., 2014 [38]
GISS-E2-R-CC	NASA GISS(USA)	1° × 1°	Schmidt et al., 2014 [38]
HadCM3	MOHC(UK)	3.75° × 2.5°	Jones et al., 2003 [39]
HadGEM2-AO	MOHC(UK)	1.875° × 1.25°	Collins et al., 2011 [40]
HadGEM2-CC	MOHC(UK)	1.875° × 1.25°	Collins et al., 2011 [40]
HadGEM2-ES	MOHC(UK)	1.875° × 1.25°	Collins et al., 2011 [40]
INM-CM4	INM(Russia)	2° × 1.5°	Volodin et al., 2010 [41]
IPSL-CM5A-LR	IPSL(France)	3.75° × 1.9°	Dufresne et al., 2013 [42]
IPSL-CM5A-MR	IPSL(France)	2.5° × 1.25°	Dufresne et al., 2013 [42]
IPSL-CM5B-LR	IPSL(France)	3.75° × 1.9°	Dufresne et al., 2013 [42]
MIROC4h	MIROC(Japan)	0.56° × 0.56°	Sakamoto et al., 2012 [43]
MIROC5	MIROC(Japan)	1.4° × 1.4°	Watanabe et al., 2010 [44]
MIROC-ESM	MIROC(Japan)	2.8° × 2.8°	Watanabe et al., 2011 [45]
MIROC-ESM-CHEM	MIROC(Japan)	2.8° × 2.8°	Watanabe et al., 2011 [45]
MPI-ESM-LR	MPI-M(Germany)	1.8° × 1.8°	Giorgetta et al., 2013 [46]
MPI-ESM-MR	MPI-M(Germany)	1.8° × 1.8°	Giorgetta et al., 2013 [46]
MPI-ESM-P	MPI-M(Germany)	1.8° × 1.8°	Giorgetta et al., 2013 [46]
MRI-CGCM3	MRI(Japan)	320 × 160 TL159	Yukimoto et al., 2012 [47]

$$D = \left\{ \frac{1}{N} \sum_{n=1}^{N} \left[\left(f_n - \bar{f} \right) - \left(r_n - \bar{r} \right) \right]^2 \right\}^{\frac{1}{2}} \quad (8)$$

Here D is used to quantify differences in the patterns of the fields f and r, while differences in the mean states of the two fields are not included. The standard deviation, correlation coefficient and RMSD are computed using climatological mean wind speeds for 1979 to 2005 and summarized using Taylor diagrams [54].

3. Results

3.1. Temporal trends of surface wind speeds

Using the NCEI-CMDC ensemble dataset, we find that wind speeds at 73% of stations have declined over the past 38 years (Fig. 1), with 67% being statistically significant ($p < 0.01$). Since only a few observations were reported in the Southern Hemisphere, we focus our study on the Northern Hemisphere and divide it into three regions: North America (20–55°N, 50–140°W), Europe (30–70°N, 20°W-50°E) and Asia (0–55°N, 50–150°E). In North America, Europe and Asia, the median wind speed trend are −0.075, −0.105 and −0.075 $ms^{-1}decade^{-1}$, respectively, which correspond to −6.5%, −9.6% and −11.2% changes over the past 38 years. China, in particular, leads the wind power industry in capacity (Table 1), and has a notable median trend of −0.110 $ms^{-1}decade^{-1}$ (-17.5% over the past 38 years). Instead of the average trend, the median trend is employed because it is more robust, and thus gives a better idea of a typical tendency within the given area. We also check the average wind speed trends and get similar results (Table 3).

The wind speed trends vary from a low to high percentile of wind speeds. Globally, wind speeds exhibit sharper trends in higher values (Fig. 2 d and Table 4), which is noteworthy because wind power generation is largely dictated by the upper percentiles of the wind speed distribution [2]. In Europe, wind speeds exhibit considerable interannual variability (Fig. 2 a). In terms of linear trends in wind speed percentiles, low percentile wind speeds show few trends, while higher wind speeds exhibit sharper downward trends. The average trend of high speed winds (90th percentile) is more than twice as large as median speed winds (50th percentile). This is also the case in Asia where high speed winds slow down much more rapidly than median speed winds (Table 4). Meanwhile, the interannual variability in Asia is rather slight, and therefore wind speed variations are dominated by long-term trends. (Fig. 2 c). In North America, interannual variability appears to be dominant because of the modest long-term trend in the wind speed time series (Fig. 2 a). Wind speeds in lower percentiles display a sharper decline than higher percentiles (Table 4). This might be an artifact caused by the introduction of the ASOS measurement in the United States in the early 1990s. The ASOS system reported higher speeds at the high end and lower speeds at the low end when compared with the former surface observation system [55].

3.2. Changes in wind power potential over the past decades

The typical height of a modern commercial wind turbine is

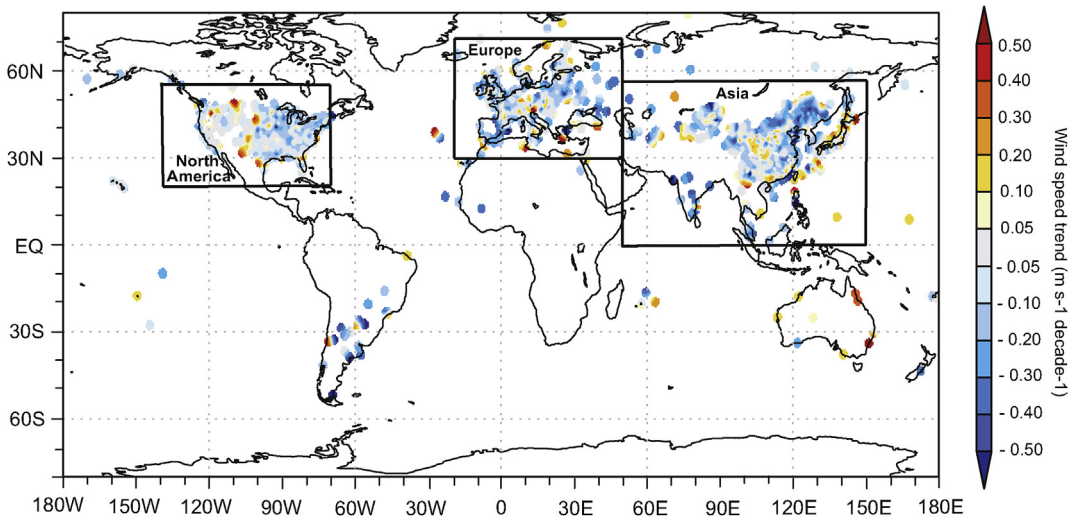

Fig. 1. Observed surface wind speed trends. The trends are computed using first degree polynomial regression for annual mean wind speeds from 1979 to 2016, expressed in $ms^{-1}decade^{-1}$. The area boundaries and the number of stations for the three regions are, North America: 20–55°N, 50–140°W, 214 stations; Europe: 30–70°N, 20°W-50°E, 224 stations; and Asia: 0–55°N, 50–150°E, 531 stations.

around 80 m while surface wind observations are around 10 m. To obtain reasonable wind power potential assessments, daily mean wind speeds at the anemometer height are extrapolated to 80 m using the power law [56]:

$$\frac{U_2}{U_1} = \left(\frac{z_2}{z_1}\right)^{\alpha} \tag{9}$$

where U_2 and U_1 are the mean wind speeds at heights z_2 and z_1, respectively. The power law index (PLI) α is an empirically-derived coefficient depending on such factors as surface roughness and atmospheric stability. For neutral stable conditions, α is approximately 0.14, which is widely applicable to low surface roughness and well-exposed sites. A number of studies pertaining to the wind energy climatology use this value [50,57–59]. This value for α is chosen for our assessments as such. Note that while the quantitative results would be sensitive to the choice of PLI or the non-neutral stability consideration in Equation (9), the trend assessment, which is the focus of this study, is lesser impacted.

The results show that a reduction in wind power potential occurs in most of the areas (Fig. 3), as deduced from analysis of section 3.1. There are 59 out of 214 (27.6%) stations in North America that have lost over 30% of their wind power potential since 1979 (Fig. 4). Stations located in Wisconsin, Kentucky, Tennessee, Louisiana, Virginia and Maine in the United States are among those which appear experienced notable impact. There are also 37 stations showing considerable growth (over 10%) in wind power potential (Fig. 4). Those stations are located in Wyoming, Montana, New

Table 3
Summary of observed surface wind speed trends. The temporal trends from previously published studies are computed by spatially averaging, expressed in $ms^{-1}decade^{-1}$. Studies listed here are selected due to the relatively large number of stations used in the analysis, and because they consider a period similar to the present study.

Source	Location	Number of stations	Duration	Temporal trends
Wan et al., 2010 [7]	Canada (42–71°N,53–136°W)	117	1953–2006	−0.05
Pryor and Ledolter, 2010 [9] [a]	the contiguous United States (25–49°N,65–125°W)	329	1973–2000	−0.19
		291		−0.19
		188	1973–2005	−0.10
		168		−0.13
Vautard et al., 2010 [20]	North America (30–75°N,50–170°W)	170	1979–2008	−0.07
Present study	North America (20–55°N,70–140°W)	214	1979–2016	−0.08
Walter et al., 2006 [10]	Germany(47–55°N, 6–15°E)	73–113[b]	1951–2001	−0.01
Brázdil et al., 2009 [11]	Czech Republic (48–51°N, 12–19°E)	23	1961–2005	−0.08
McVicar et al., 2010 [13]	Switzerland (46–48°N, 6–10°E)	25	1983–2006	−0.09
Najac et al., 2011 [12], McVicar et al., 2012 [8]	France (43–51°N, 5°W-8°E)	51	1984–2003	−0.05
Papaioannou et al., 2011 [14]	Greece (35–41°N, 20–28°E)	20	1959–2001	−0.01
Vautard et al., 2010 [20]	Europe (30–75°N,20°W-40°E)	276	1979–2008	−0.09
Present study	Europe (30–70°N,20°W-50°E)	224	1979–2016	−0.105
Fujibe, 2009 [16]	Japan (31–46°N, 129–146°E)	327	1979–2008	−0.03
Bandyopadhyay et al., 2009 [15]	India (9–34°N, 69–95°E)	133	1971–2002	−0.27
Guo et al., 2011 [18]	P.R. China (18–54°N,73–135°E)	652	1969–2005	−0.18
Yin et al., 2010 [19]		603	1971–2008	−0.12
Chen et al., 2013 [17]		540	1971–2007	−0.17
Present study		351	1979–2016	−0.13
Vautard et al., 2010 [20]	Central Asia (30–75°N,40–100°E)	96	1979–2008	−0.16
	Eastern Asia (30–75°N,100–160°E)	190	1979–2008	−0.12
Present study	Asia (0–55°N,50–150°E)	531	1979–2016	−0.10

[a] Temporal trends in this study are spatial median values, while all other studies are spatial average.
[b] 1 km resolution monthly grid using 73–113 sites per month.

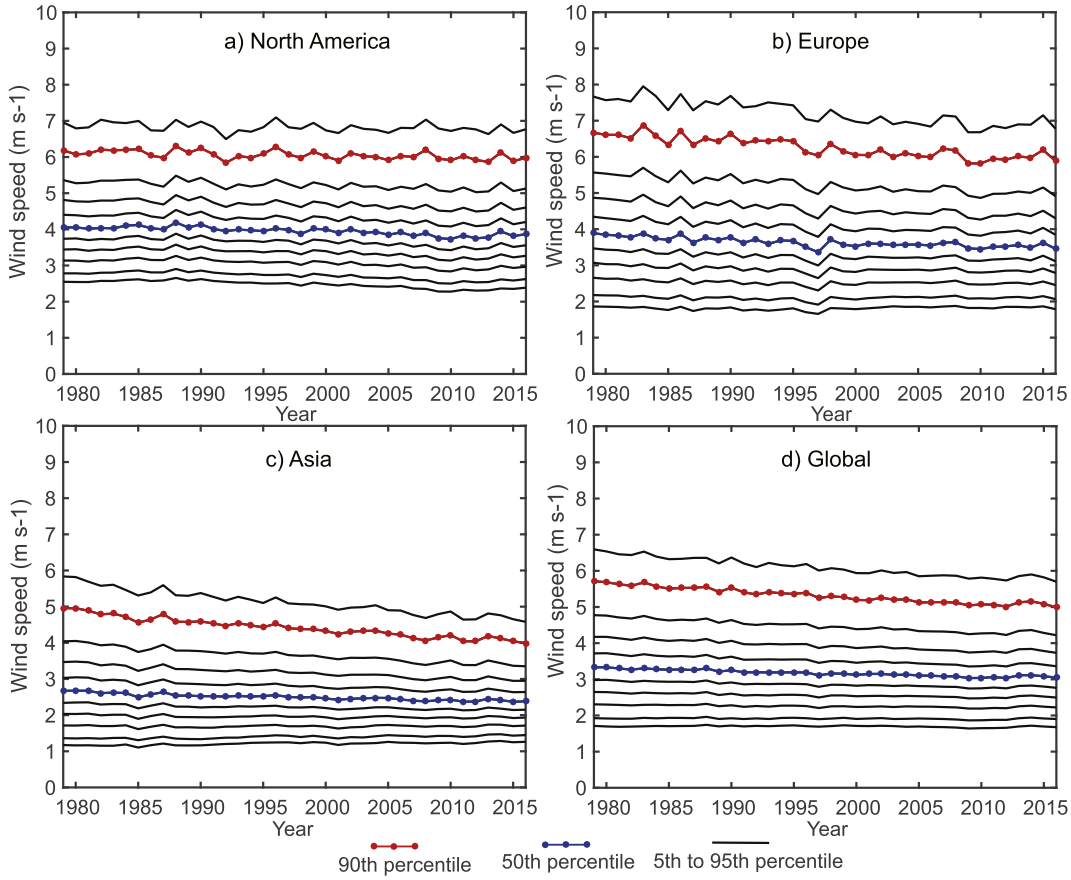

Fig. 2. Percentile wind speed trend. Evolution, as a function of year, of annual percentile for observed surface wind speeds. 5th, 10th - 90th in 10 percentile increment and 95th percentile are shown. The domain considered for a)North America, b)Europe, c)Asia is the same as in Fig. 1, while d)Global considers all the sites available in the dataset.

Table 4
Surface wind speed trends for different percentiles. Trends are computed using first degree polynomial regression for annual wind speed percentiles for the period 1979 to 2016, in $ms^{-1}decade^{-1}$[a]. The domain considered for North America, Europe and Asia is the same as that in Fig. 1, while d)Global considers all the all sites available in the dataset.

	North America	Europe	Asia	Global
5th	**−0.084**	0.008	**0.028**	**−0.010**
10th	**−0.084**	−0.006	**0.027**	**−0.008**
20th	**−0.083**	**−0.028**	0.003	**−0.023**
30th	**−0.082**	**−0.049**	**−0.021**	**−0.040**
40th	**−0.082**	**−0.071**	**−0.047**	**−0.057**
50th	**−0.082**	**−0.093**	**−0.074**	**−0.076**
60th	**−0.081**	**−0.114**	**−0.101**	**−0.095**
70th	**−0.078**	**−0.141**	**−0.134**	**−0.118**
80th	**−0.072**	**−0.171**	**−0.174**	**−0.177**
90th	**−0.057**	**−0.218**	**−0.237**	**−0.184**
95th	−0.040	**−0.261**	**−0.296**	**−0.222**

[a] Bold values denote that the trends are significant ($p < 0.01$).

Mexico, Texas, South Dakota, Nebraska and Florida in the United States (Fig. 3 a). In Europe, wind power potential in 118 out of 224 (52.7%) stations have decreased by more than 30%. Meanwhile, only 25 stations have a more than 10% increase (Fig. 4). Stations having the sharpest reduction are located in the Republic of Belarus, central France and Ireland, while stations in northern Italy, western Switzerland and western Austria show considerable growth(Fig. 3 b). Notably, France and Italy are among the top five countries in terms of installed wind power capacity in Europe and among the top 10 in the world [3] (Table 1). Among the 12 stations located on the African continent, half of them display a 30% decrease in wind power potential or more, while only two document a 30% increase or more. There are four out of five stations in Morocco with a significant decline, however, the three Tunisian stations show a slight or even significant increase. One Egyptian station has a remarkable decrease, while the other shows a slight increase. The remaining two African continental stations are located in Mauritania and they

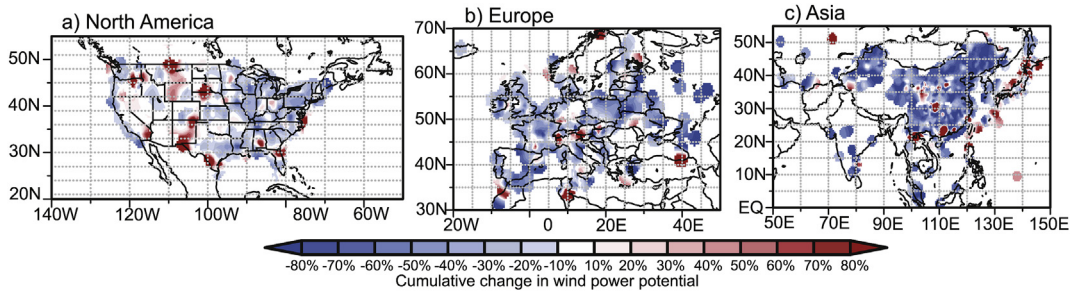

Fig. 3. Spatial distribution of cumulative changes in wind power potential. Cumulative changes over a)North America, b)Europe and c)Asia from 1979 to 2016.

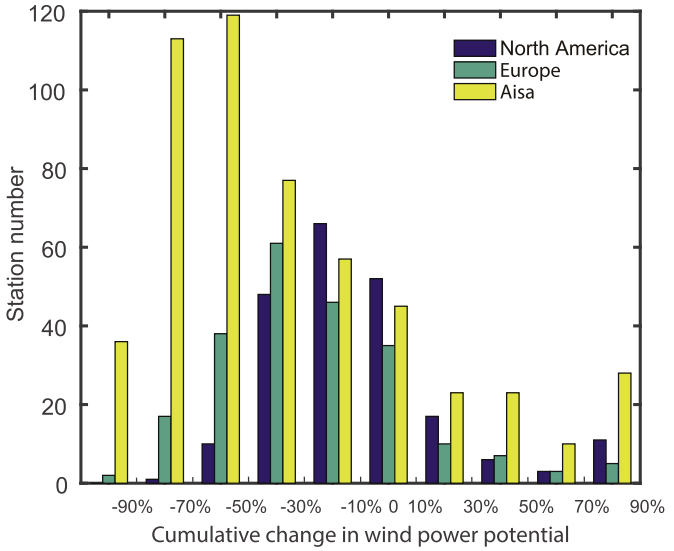

Fig. 4. Frequency distribution of cumulative changes in wind power potential. Cumulative changes in the wind power potential from 1979 to 2016. The domain for North America, Europe and Asia is the same as that in Fig. 1.

both exhibit a considerable decrease in wind power potential. Remarkable alterations occur in Asia, where 65.0% of the stations show more than a 30% decrease with 50.5% with more than a 50% decrease (Fig. 4). Since most of the accessible stationary observations in Asia were collected in three of the leading countries in wind energy generation (P.R. China, India and Japan: see Table 1), we focus our discussion on these three countries. There are 276 out of 351 (78.6%) stations in China that lost more than 30% of their wind power potential over the past decades. A significant decrease in wind power potential occurs in the northwest and northeast regions of China, whereas stations with an increase in wind power potential are scattered around the central and southeast coast (Fig. 3 c). For all 10 Indian stations included in the study, nine have a considerable decrease in wind energy resource with a median change of −70%. This result is remarkable but reasonable considering an extreme trend of $-0.27\ ms^{-1}decade^{-1}$ was reported in India using observations for 1971–2002 derived from 133 stations (Table 3). Nevertheless, Japan seems to be an exception in this widespread stilling, where an increase in wind power potential was discovered in almost half of the stations (51 out of 103), most of which are located in Hokkaido, and the northern and western coastal of Honshu (Fig. 3 c).

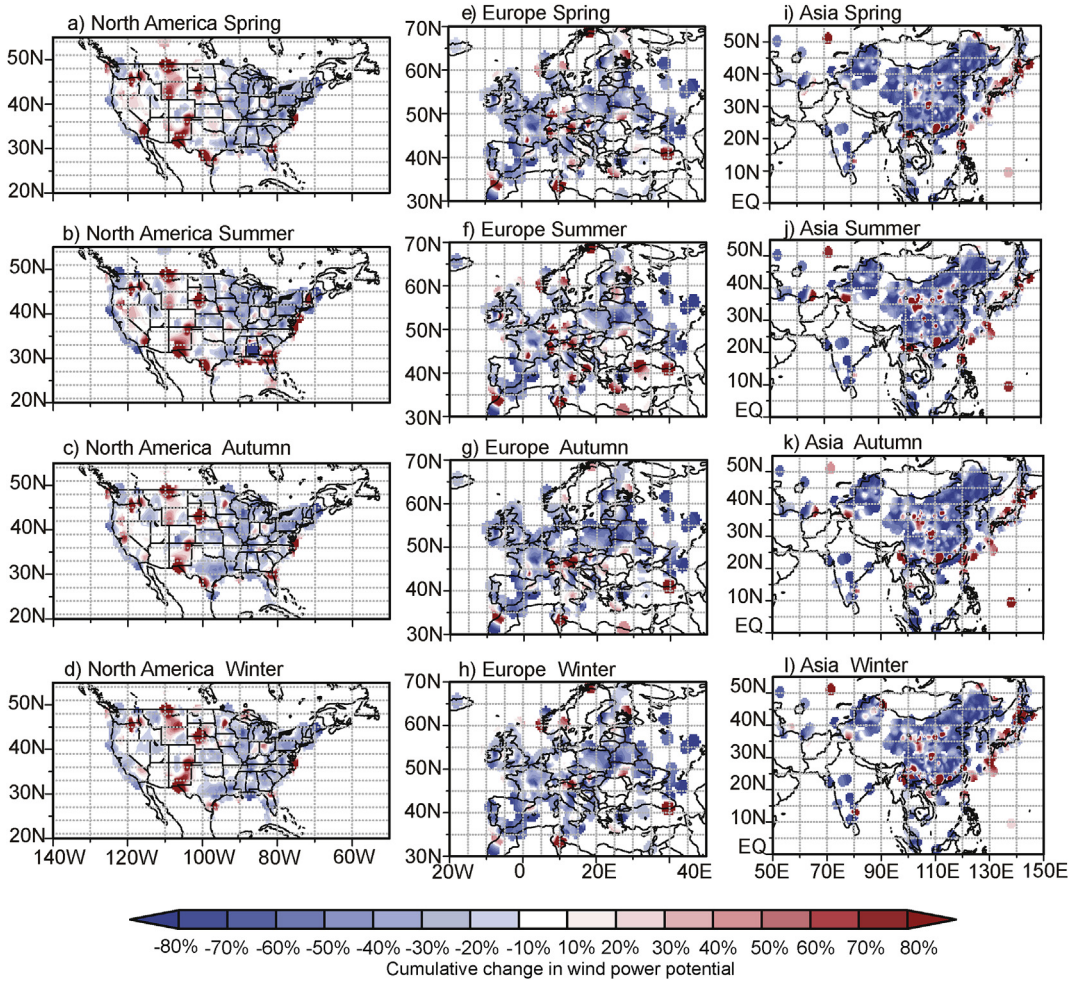

Fig. 5. Seasonal cumulative changes in wind power potential. Computation of cumulative changes is the same as in Fig. 3, except using seasonal mean values rather than annual mean. The three columns correspond to North America, Europe, and Asia. The four seasons: Spring (Mar, Apr & May), Summer (Jun, Jul & Aug.), Autumn (Sept, Oct & Nov), and Winter (Dec, Jan & Feb) patterns are shown in the four rows for each of the continents.

Table 5
CMIP5 historical simulations of surface winds. The spatial median speeds corresponding to every model are computed using temporal mean speeds for 1979–2005, in ms^{-1}, and the spatial median trends are computed using temporal trends for 1979–2005, expressed in $ms^{-1}decade^{-1}$. The heights are vertical coordinates of model outputs, expressed in *m*.

Indicator	Model Name	Height	Median speed	Median trend[a]
B	ACCESS1.0	10	2.99	−1.18
C	ACCESS1.3	10	3.32	−6.44
D	BCC-CSM1.1	10	4.92	12.0
E	BCC-CSM1.1(m)	10	4.39	5.71
F	BNU-ESM	10	4.391	−7.26
G	CanESM2	10	4.98	2.75
H	CMCC-CESM	10	3.65	5.88
I	CMCC-CM	10	3.52	−8.08
J	CMCC-CMS	10	3.56	−8.55
K	CSIRO-Mk3.6.0	2	2.02	−8.57
L	FGOALS-s2	10	3.84	16.0
M	GFDL-CM3	10	3.34	3.28
N	GFDL-ESM2G	10	3.31	−4.82
O	GFDL-ESM2M	10	3.16	3.03
P	GISS-E2-H	10	3.20	−9.02
Q	GISS-E2-H-CC	10	3.18	−6.08
R	GISS-E2-R	10	3.35	−4.63
S	GISS-E2-R-CC	10	3.34	−7.94
T	HadCM3	10	3.87	−3.74
U	HadGEM2-AO	10	2.95	−5.10
V	HadGEM2-CC	10	2.91	3.41
W	HadGEM2-ES	10	2.91	−14.0
X	INM-CM4	10	3.61	8.32
Y	IPSL-CM5A-LR	10	3.27	10.0
Z	IPSL-CM5A-MR	10	3.30	−5.66
a	IPSL-CM5B-LR	10	3.48	−5.81
b	MIROC4h	10	2.70	−1.60
c	MIROC5	10	3.51	−27.0
d	MIROC-ESM	10	3.30	−9.25
e	MIROC-ESM-CHEM	10	3.36	−10.0
f	MPI-ESM-LR	10	3.94	20.0
g	MPI-ESM-MR	10	3.91	1.70
h	MPI-ESM-P	10	3.84	13.0
i	MRI-CGCM3	10	3.27	12.0
A	**Observation**	**10**	**3.40**	**−95.0**

[a] All median trends have been multiplied by 10^4.

Since wind power potential varies greatly among seasons, it is necessary to examine seasonal changes and their differences. The results show that a widespread decline in wind power potential appears for all seasons in the Northern Hemisphere (Fig. 5), with the comparable magnitude. The largest median decrease rate occurs in the season with the largest median wind power potential in Asia (spring), as well as in North America (winter). In northwest region of China, the strongest decline occurs in the spring (Fig. 5 i-l). Since spring is also the season with the largest mean wind speed in China [18], it can have a substantial impact on Chinese wind energy generation. In Texas, the leading state in the wind energy industry in terms of installed capacity in the United States, wind power potential declines more rapidly in the autumn and winter (Fig. 5 a-d). However, the largest median decrease rate in Europe occurs in the autumn (the season with the 3rd largest median wind power potential) exceeded by winter and spring. In Germany, the largest wind energy generating country in Europe, downward trends are sharper in the autumn and winter, during which hardly any regions have a considerable increase (Fig. 5 e-h).

3.3. Evaluation of CMIP5 simulations on surface wind speeds

The most straightforward approach to evaluate model performances is by comparing simulated quantities with corresponding observationally-based estimates [60]. Herein, CMIP5 simulations of surface wind speeds for 1979 to 2005 over the Northern Hemisphere are quantified and compared with the observations. In order to evaluate model simulations on wind speed climatology, the spatial median value for every model is computed using climatological mean wind speeds. The results show that among the 34 models included in this study, 14 of them are highly consistent (the difference in median values being less than 0.17 ms^{-1}, which account for 5% of the observations) with the observation. However, there are 6 models that exhibit a large bias (the difference in median values being more than 0.7 ms^{-1}, accounting for 20% of the observations): MIROC4h, CSIRO-Mk3.6.0, BCC-CSM1.1, BNU-ESM, BCC-CSM1.1(m) and CanESM2 (Table 5). It is worthy to note that surface wind speeds of CSIRO-Mk3.6.0 are reported at 2 m, while for all other models, they are obtained at 10 m.

In terms of long-term trends, 18 out of 28 models (those with a large bias in median wind speed, i.e., BCC-CMS1.1, BCC-CMS1.1(m), BNU-ESM, CanESM2, CSIRO-Mk3.6.0 and MIROC4h are excluded) exhibit negative median trends while the other 10 models exhibit positive values as shown in Fig. 6. Unfortunately, none of the AOGCM-simulated median wind speed trends are of the same magnitude as the observational value (Table 5). Even for the model with the sharpest decline: MIROC5, the rate of change is less than 30% of the observation. A similar conclusion can be drawn in anomalies (Fig. 7), indicating that the CMIP5 models included in the study have a challenge in simulating long-term changes in wind speeds. Another study [61] analyzing the CMIP3 results, it was reported that those models also perform poorly in terms of climate models' ability to reproduce recent trend in the observations.

The standard deviation, correlation coefficient and RMSD of model simulations for climatological mean states from 1979 to 2005 are computed and summarized in Fig. 8. The results show that wind speeds from a number of models correlated well with the observations of spatial patterns (e.g., ACCESS1.0, CanESM2, CMCC-CM and HadGEM2-ES), while some other model outputs are poorly correlated with observed wind speeds (e.g. FGOALS-s2 and BCC-CSM1.1(m)). The correlation coefficients between model simulations and observation are mostly between 0.3 and 0.6 with 13 values larger than 0.5. As for RMSD, most of the models (24 out of 34) range from 1 to 1.5. ACCESS1.0, CanESM2, CMCC-CM and GFDL-ESM2G are the models with relatively small values, suggesting that they are the ones most similar in pattern to the observations. However, the RMSD values for MIROC-ESM and MIROC-ESM-CHEM are far larger than the other models (see Fig. 8), indicating modest performance in reproducing wind speed patterns for the historical period.

4. Conclusion and discussion

Wind energy is one of the most commonly used renewable energy around the world and is hugely beneficial to climate change mitigation. A comprehensive analysis on changes of wind power potential in recent decades is conducted in the current study, with the propose of addressing concerns regarding the possible impact of atmospheric stilling on wind energy resources. Unlike most previous studies focusing on a regional domain, this study conduct analysis on a hemisphere scale covering North America, Europe and Asia.

The results from analysis of observational surface wind speeds reemphasize that atmospheric stilling is a widespread and potentially global phenomenon. Among the three continents included in this study, the decline in Asia is much sharper compared to North America and Europe. In terms of wind speed percentiles, strong winds decline faster than weak winds in Asia and Europe, while in North America, weak winds exceed strong winds in decline ratio.

Consistent with the decrease of surface wind speeds, the wind power potential was also decreasing in most regions of the

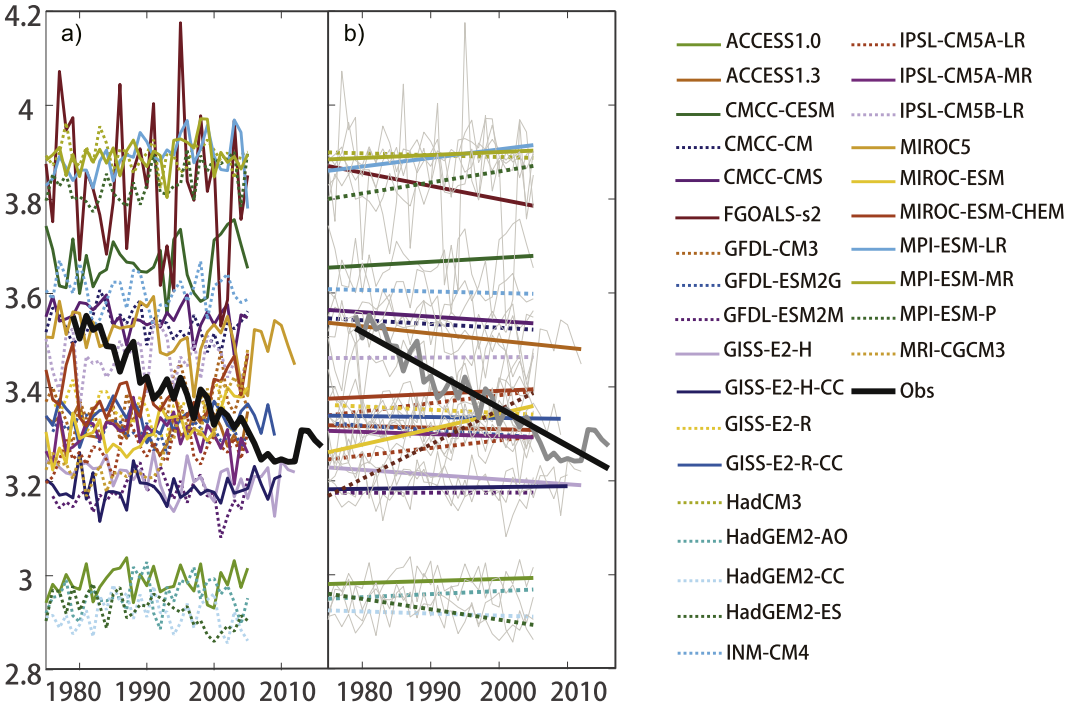

Fig. 6. Evolution of CMIP5 simulated surface wind speeds. a) Evolution, as a function of year, of median values of surface wind speeds simulated by 28 AOGCMs in CMIP5. b) Trendline for the surface wind speeds. 17 models exhibit downward trends while the remaining models show upward trends. Evolution of the median values for the observation winds are also shown.

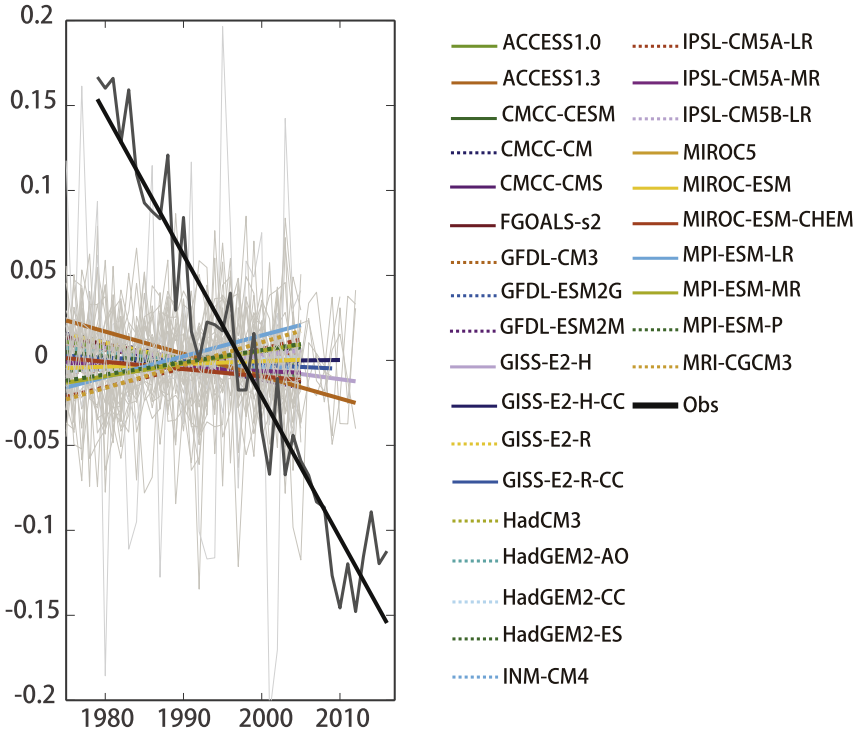

Fig. 7. Evolution of CMIP5 simulated surface wind speed anomalies. Same as Fig. 6 b), but for surface wind speed anomalies.

Northern Hemisphere in the past decades. Around one third of the stations in North America, have experienced a huge decrease (over 30%) in wind power potential while over half of the stations in Europe and around four-fifths in Asia have the same magnitude of decrease. For China, the country with the largest installed wind energy capacity, regions which have a considerable decrease are mainly regions with abundant wind energy resources and where a number of gigantic commercial wind farms were built. Changes in

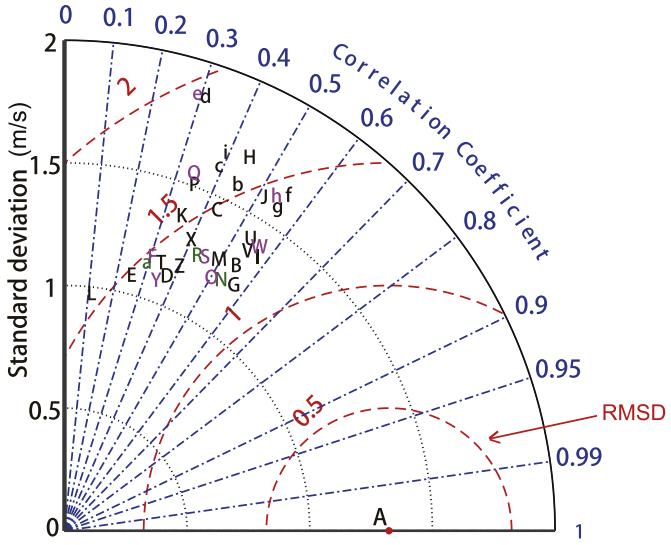

Fig. 8. Taylor diagram of CMIP5 simulated surface wind speeds. Each of the 35 letters denotes a 1979–2005 temporal mean surface wind field, among which A denotes the observation while B-Z and a-i denotes each of the 34 model simulation field. The letters correspond to the models listed in Table 5. The radial distance from the origin is proportional to the standard deviation of a surface wind climatology. The RMSD between the model (shown by arcs) and the observation fields are proportional to their distance. The correlation between the model simulation and observation fields are given by the azimuthal position of the model simulation fields. So for example, point 'd' indicates MIROC-ESM model. Whose RMSD is close to 2, and correlation coefficient is between 0.3 and 0.4 m with standard deviation of wind speed between 1.5 and 2 m/s.

all four seasons are of the similar magnitude despite the large differences in their mean states. For Asia and North America, the sharpest decrease appears along with the largest mean wind power potential. However, this is not the case for Europe, where the sharpest decrease in wind power potential appears in the autumn, while the largest mean value occurs in the winter.

We evaluated the skill of the CMIP5 models in simulating the changes in surface wind speeds. No model could replicate the Northern Hemisphere median long-term trends of surface wind speeds. Model outputted wind speeds exhibit either a slight increase or a slight decrease in recent decades, in contrast to a significant decline in the observations. The pattern of climatological wind speeds in CMIP5 simulations is also not consistent with the observations compared to the surface temperature simulation [62]. Thus the CMIP5 simulations of the changes in surface wind speeds should be used with considerable caution and likely not reliable. Hence, wind energy projections based on CMIP5 surface wind speed simulations should also be used with careful consideration to the model performance.

It is worthy to note that historical wind speed trends cannot be simply interpreted as a likely future outcome since wind speed trends are subject to complicated internal variability and external forcings. Large-scale climate modes of variability, such as the ENSO, Pacific Decadal Oscillation (PDO) and North Atlantic Oscillation (NAO) have a large impact on regional or global climate [63–65]. These internal climate modes may manifest as large-scale temporal trends in wind climate [66], but how they will evolve in the future is still uncertain. There are also meso (regional) scale land changes that can affect the surface roughness and winds. Therefore, it is a challenge to project a future scenario using historical records.

There remain continuing uncertainties associated with the coverage of surface wind observations and the vertical extrapolation algorithm. Although data from more than 1000 surface stations have been included, there are still places with limited coverage of our analysis in places such as Africa, the Middle East and also high latitude Asia and North America (see Fig. 1). These places either have a lack of surface stations or their observation records did not qualify for our climatological study. Therefore, uncertainties remain in the tropical and polar regions. The extrapolation algorithm we adopt, namely the power law, is a empirical wind speed profile and the index varies from different terrains and wind speeds. Although long-term trends are less sensitive to the choice of profile power law term, they might still have been amplified or diminished. We tested a sample with two values PLI = 0.14 (as used in this study) and an exaggerated value of PLI = 0.25. The corresponding trends were nearly identical with some extreme wind values exhibiting difference if any.

Overall, the study finds systematic wind "stilling" in many parts of the Northern Hemisphere. The climate models have high uncertainty in their ability to simulate the surface winds. This challenge should be addressed by better boundary layer, land-atmosphere interaction considerations. Tests are also needed regarding difference vertical scaling approaches for wind profiles.

Acknowledgement

Surface observed wind speeds were downloaded from the website of the National Centers for Environmental Information (NCEI) at https://www.ncdc.noaa.gov/isd and the website of the China Meteorological Data Service Center (CMDC) at http://data.cma.cn/data/detail/dataCode/SURF_CLI_CHN_MUL_DAY_V3.0/keywords/v3.0.html. We acknowledge these groups for making the observational data available. The AOGCM data used were obtained from the data portal developed for the 5th Assessment Report of the Intergovernmental Panel on Climate Change. We thank the international modeling groups for providing their modeling data and the Program for Climate Model Diagnosis and Intercomparison (PCMDI) for collecting and archiving the model data. We acknowledge financial support from the National Key R&D Program of China (2018YFA0605904), the National Natural Science Foundation of China (41831175, 41425019, 41721004, 41661144016 and 41775086), Strategic Priority Research Program of Chinese Academy of Sciences (XDA20060501), State Key Laboratory of Tropical Oceanography, South China Sea Institute of Oceanology, Chinese Academy of Sciences (LTO1704). Qun Tian acknowledges financial support from the China Scholarship Council during his visit to Purdue University, USA. Qun Tian thanks Dr. Xi Luo for her love and support.

References

[1] Sawin JL, Sverrisson F, Seyboth K, Adib R, Murdock HE, Lins C, Edwards I, Hullin M, Nguyen LH, Prillianto SS, et al. Renewables 2017 global status report. Tech. Rep. Renewable Energy Policy Network for the 21st Century; 2017. http://www.ren21.net/gsr-2017/.

[2] Pryor S, Barthelmie R. Climate change impacts on wind energy: a review. Renew Sustain Energy Rev 2010;14(1):430–7.

[3] Sawyer S, Dyrholm M. Global wind report. Annual market update 2016. Tech. Rep. Global Wind Energy Council; 2017. http://gwec.net/publications/global-wind-report-2/global-wind-report-2016/.

[4] Carvalho D, Rocha A, Gómez-Gesteira M, Santos CS. Potential impacts of climate change on European wind energy resource under the CMIP5 future climate projections. Renew Energy 2017;101:29–40.

[5] Manwell JF, McGowan JG, Rogers AL. Wind energy explained: theory, design and application. John Wiley & Sons; 2010.

[6] M. L. Roderick, L. D. Rotstayn, G. D. Farquhar, M. T. Hobbins, On the attribution of changing pan evaporation, Geophys Res Lett 34 (17). doi:10.1029/2007GL031166.

[7] Wan H, Wang XL, Swail VR. Homogenization and trend analysis of Canadian near-surface wind speeds. J Clim 2010;23(5):1209–25.

[8] McVicar TR, Roderick ML, Donohue RJ, Li LT, Van Niel TG, Thomas A, Grieser J, Jhajharia D, Himri Y, Mahowald NM, et al. Global review and synthesis of trends in observed terrestrial near-surface wind speeds: implications for evaporation. J Hydrol 2012;416:182–205.

[9] S. Pryor, J. Ledolter, Addendum to "Wind speed trends over the contiguous United States", J Geophys Res: Atmos 115 (D10).
[10] Walter A, Keuler K, Jacob D, Knoche R, Block A, Kotlarski S, Müller-Westermeier G, Rechid D, Ahrens W. A high resolution reference data set of German wind velocity 1951–2001 and comparison with regional climate model results. Meteorol Z 2006;15(6):585–96.
[11] Brázdil R, Chromá K, Dobrovolnỳ P, Tolasz R. Climate fluctuations in the Czech Republic during the period 1961–2005. Int J Climatol 2009;29(2):223–42.
[12] Najac J, Lac C, Terray L. Impact of climate change on surface winds in France using a statistical-dynamical downscaling method with mesoscale modelling. Int J Climatol 2011;31(3):415–30.
[13] T. R. McVicar, T. G. Van Niel, M. L. Roderick, L. T. Li, X. G. Mo, N. E. Zimmermann, D. R. Schmatz, Observational evidence from two mountainous regions that near-surface wind speeds are declining more rapidly at higher elevations than lower elevations: 1960–2006, Geophys Res Lett 37 (6).
[14] G. Papaioannou, G. Kitsara, S. Athanasatos, Impact of global dimming and brightening on reference evapotranspiration in Greece, J Geophys Res: Atmos 116 (D9).
[15] Bandyopadhyay A, Bhadra A, Raghuwanshi N, Singh R. Temporal trends in estimates of reference evapotranspiration over India. J Hydrol Eng 2009;14(5):508–15.
[16] Fujibe F. Relation between long-term temperature and wind speed trends at surface observation stations in Japan. SOLA 2009;5:81–4.
[17] Chen L, Li D, Pryor S. Wind speed trends over China: quantifying the magnitude and assessing causality. Int J Climatol 2013;33(11):2579–90.
[18] Guo H, Xu M, Hu Q. Changes in near-surface wind speed in China: 1969–2005. Int J Climatol 2011;31(3):349–58.
[19] Yin Y, Wu S, Dai E. Determining factors in potential evapotranspiration changes over China in the period 1971–2008. Chin Sci Bull 2010;55(29):3329–37.
[20] Vautard R, Cattiaux J, Yiou P, Thépaut J-N, Ciais P. Northern Hemisphere atmospheric stilling partly attributed to an increase in surface roughness. Nat Geosci 2010;3(11):756.
[21] Taschetto AS, Gupta AS, Jourdain NC, Santoso A, Ummenhofer CC, England MH. Cold tongue and warm pool ENSO events in CMIP5: mean state and future projections. J Clim 2014;27(8):2861–85.
[22] Taylor KE, Stouffer RJ, Meehl GA. An overview of CMIP5 and the experiment design. Bull Am Meteorol Soc 2012;93(4):485–98.
[23] L. Chen, S. Pryor, D. Li, Assessing the performance of Intergovernmental Panel on Climate Change AR5 climate models in simulating and projecting wind speeds over China, J Geophys Res: Atmos 117 (D24) .
[24] S. Pryor, R. Barthelmie, D. Young, E. S. Takle, R. W. Arritt, D. Flory, W. Gutowski, A. Nunes, J. Roads, Wind speed trends over the contiguous United States, J Geophys Res: Atmos 114 (D14).
[25] Smith A, Lott N, Vose R. The integrated surface database: recent developments and partnerships. Bull Am Meteorol Soc 2011;92(6):704–8.
[26] Flannery BP, Teukolsky SA, Press WH, Vetterling WT. Numerical recipes in C: the art of scientific computing, vol. 2. Cambridge University Press; 1988.
[27] Dix M, Vohralik P, Bi D, Rashid H, Marsland S, OFarrell S, Uotila P, Hirst T, Kowalczyk E, Sullivan A, et al. The access coupled model: documentation of core CMIP5 simulations and initial results. Aust Meteorol Oceanogr J 2013;63(1):83–99.
[28] Xin X, Zhang L, Zhang J, Wu T, Fang Y. Climate change projections over East Asia with BCC_CSM1. 1 climate model under RCP scenarios. J Meteorol Soc Jpn Ser II 2013;91(4):413–29.
[29] Liu X, Wu T, Yang S, Jie W, Nie S, Li Q, Cheng Y, Liang X. Performance of the seasonal forecasting of the Asian summer monsoon by BCC_CSM1. 1 (m). Adv Atmos Sci 2015;32(8):1156–72.
[30] Ji D, Wang L, Feng J, Wu Q, Cheng H, Zhang Q, Yang J, Dong W, Dai Y, Gong D, et al. Description and basic evaluation of Beijing Normal University Earth system model (BNU-ESM) version 1. Geosci Model Dev (GMD) 2014;7(5):2039–64.
[31] V. Arora, J. Scinocca, G. Boer, J. Christian, K. Denman, G. Flato, V. Kharin, W. Lee, W. Merryfield, Carbon emission limits required to satisfy future representative concentration pathways of greenhouse gases, Geophys Res Lett 38 (5). doi:10.1029/2010GL046270.
[32] Fogli PG, Manzini E, Vichi M, Alessandri A, Patara L, Gualdi S, Scoccimarro E, Masina S, Navarra A. INGV-CMCC carbon (ICC): a carbon cycle earth system model. CMCC Res Pap 2009;61:31.
[33] Gordon HB, O'Farrell S, Collier M, Dix M, Rotstayn L, Kowalczyk E, Hirst T, Watterson I. The CSIRO Mk3. 5 climate model. CSIRO and Bureau of Meteorology; 2010.
[34] Bao Q, Lin P, Zhou T, Liu Y, Yu Y, Wu G, He B, He J, Li L, Li J, et al. The flexible global ocean-atmosphere-land system model, spectral version 2: FGOALS-s2. Adv Atmos Sci 2013;30(3):561–76.
[35] Griffies SM, Winton M, Donner LJ, Horowitz LW, Downes SM, Farneti R, Gnanadesikan A, Hurlin WJ, Lee H-C, Liang Z, et al. The GFDL CM3 coupled climate model: characteristics of the ocean and sea ice simulations. J Clim 2011;24(13):3520–44.
[36] Dunne JP, John JG, Adcroft AJ, Griffies SM, Hallberg RW, Shevliakova E, Stouffer RJ, Cooke W, Dunne KA, Harrison MJ, et al. GFDLs ESM2 global coupled climate–carbon earth system models. Part I: physical formulation and baseline simulation characteristics. J Clim 2012;25(19):6646–65.
[37] Dunne JP, John JG, Shevliakova E, Stouffer RJ, Krasting JP, Malyshev SL, Milly P, Sentman LT, Adcroft AJ, Cooke W, et al. GFDLs ESM2 global coupled climate–carbon earth system models. Part II: carbon system formulation and baseline simulation characteristics. J Clim 2013;26(7):2247–67.
[38] Schmidt GA, Kelley M, Nazarenko L, Ruedy R, Russell GL, Aleinov I, Bauer M, Bauer SE, Bhat MK, Bleck R, et al. Configuration and assessment of the GISS ModelE2 contributions to the CMIP5 archive. J Adv Model Earth Syst 2014;6(1):141–84.
[39] Johns T, Gregory J, Ingram W, Johnson C, Jones A, Lowe J, Mitchell J, Roberts D, Sexton D, Stevenson D, et al. Anthropogenic climate change for 1860 to 2100 simulated with the HadCM3 model under updated emissions scenarios. Clim Dynam 2003;20(6):583–612.
[40] Collins W, Bellouin N, Doutriaux-Boucher M, Gedney N, Halloran P, Hinton T, Hughes J, Jones C, Joshi M, Liddicoat S, et al. Development and evaluation of an Earth-System model-HadGEM2. Geosci Model Dev (GMD) 2011;4(4):1051.
[41] Volodin E, Dianskii N, Gusev A. Simulating present-day climate with the INMCM4. 0 coupled model of the atmospheric and oceanic general circulations. Izvestiya Atmos Ocean Phys 2010;46(4):414–31.
[42] Dufresne J-L, Foujols M-A, Denvil S, Caubel A, Marti O, Aumont O, Balkanski Y, Bekki S, Bellenger H, Benshila R, et al. Climate change projections using the IPSL-CM5 earth system model: from CMIP3 to CMIP5. Clim Dynam 2013;40(9–10):2123–65.
[43] Sakamoto TT, Komuro Y, Nishimura T, Ishii M, Tatebe H, Shiogama H, Hasegawa A, Toyoda T, Mori M, Suzuki T, et al. MIROC4h–a new high-resolution atmosphere-ocean coupled general circulation model. J Meteorol Soc Jpn Ser II 2012;90(3):325–59.
[44] Watanabe M, Suzuki T, Oishi R, Komuro Y, Watanabe S, Emori S, Takemura T, Chikira M, Ogura T, Sekiguchi M, et al. Improved climate simulation by MIROC5: mean states, variability, and climate sensitivity. J Clim 2010;23(23):6312–35.
[45] Watanabe S, Hajima T, Sudo K, Nagashima T, Takemura T, Okajima H, Nozawa T, Kawase H, Abe M, Yokohata T, et al. MIROC-ESM 2010: model description and basic results of CMIP5-20c3m experiments. Geosci Model Dev (GMD) 2011;4(4):845.
[46] Giorgetta MA, Jungclaus J, Reick CH, Legutke S, Bader J, Böttinger M, Brovkin V, Crueger T, Esch M, Fieg K, et al. Climate and carbon cycle changes from 1850 to 2100 in MPI-ESM simulations for the Coupled Model Intercomparison Project phase 5. J Adv Model Earth Syst 2013;5(3):572–97.
[47] Yukimoto S, Adachi Y, Hosaka M, Sakami T, Yoshimura H, Hirabara M, Tanaka TY, Shindo E, Tsujino H, Deushi M, et al. A new global climate model of the Meteorological Research Institute: MRI-CGCM3–model description and basic performance–. J Meteorol Soc Japan Ser II 2012;90:23–64.
[48] Mirhosseini M, Sharifi F, Sedaghat A. Assessing the wind energy potential locations in province of Semnan in Iran. Renew Sustain Energy Rev 2011;15(1):449–59.
[49] Zheng C, Pan J. Assessment of the global ocean wind energy resource. Renew Sustain Energy Rev 2014;33:382–91.
[50] Islam M, Saidur R, Rahim N. Assessment of wind energy potentiality at Kudat and Labuan, Malaysia using Weibull distribution function. Energy 2011;36(2):985–92.
[51] Katsoulis B. A survey on the assessment of wind energy potential in Greece. Theor Appl Climatol 1993;47(1):51–63.
[52] Qing X. Statistical analysis of wind energy characteristics in Santiago island, Cape Verde. Renew Energy 2018;115:448–61.
[53] Soulouknga MH, Doka SY, Revanna N, Djongyang N, Kofane TC. Analysis of wind speed data and wind energy potential in Faya-Largeau, Chad, using Weibull distribution. Renew Energy 2018;121:1–8.
[54] Taylor KE. Summarizing multiple aspects of model performance in a single diagram. J Geophys Res: Atmos 2001;106(D7):7183–92.
[55] T. B. McKee, N. J. Doesken, C. A. Davey, R. A. Pielke Sr, reportClimate data continuity with ASOS: Report for period April 1996 through June 2000, climatology report; 00-3. URL https://mountainscholar.org/bitstream/handle/10217/169847/CLMR_Climatology00-3.pdf?sequence=1.
[56] Mayhoub A, Azzam A. A survey on the assessment of wind energy potential in Egypt. Renew Energy 1997;11(2):235–47.
[57] Peterson EW, Hennessey Jr JP. On the use of power laws for estimates of wind power potential. J Appl Meteorol 1978;17(3):390–4.
[58] Argeso D, Businger S. Wind power characteristics of Oahu, Hawaii. Renew Energy 2018;128:324–36. https://doi.org/10.1016/j.renene.2018.05.080. http://www.sciencedirect.com/science/article/pii/S0960148118306013.
[59] Wang J, Hu J, Ma K. Wind speed probability distribution estimation and wind energy assessment. Renew Sustain Energy Rev 2016;60:881–99. https://doi.org/10.1016/j.rser.2016.01.057. http://www.sciencedirect.com/science/article/pii/S1364032116000873.
[60] Flato G, Marotzke J, Abiodun B, Braconnot P, Chou SC, Collins WJ, Cox P, Driouech F, Emori S, Eyring V, et al. Evaluation of climate models. In: Climate change 2013: the physical science basis. Contribution of working group I to the fifth assessment Report of the intergovernmental Panel on climate change, climate change, vol. 5; 2013. p. 741–866. 2013.
[61] Jiang Y, Luo Y, Zhao Z. Evaluation of wind speeds in China as simulated by global climate models. Acta Meteorol Sin 2009;67(06):923–34.
[62] Jones GS, Stott PA, Christidis N. Attribution of observed historical near–surface temperature variations to anthropogenic and natural causes using CMIP5 simulations. J Geophys Res: Atmos 2013;118(10):4001–24.
[63] Hu K, Huang G, Zheng X-T, Xie S-P, Qu X, Du Y, Liu L. Interdecadal variations in ENSO influences on Northwest Pacific–East Asian early summertime climate simulated in CMIP5 models. J Clim 2014;27(15):5982–98.

[64] Mantua NJ, Hare SR. The pacific decadal oscillation. J Oceanogr 2002;58(1):35–44.
[65] Hurrell JW, Kushnir Y, Ottersen G, Visbeck M. An overview of the north Atlantic oscillation, the North Atlantic oscillation: climatic significance and environmental impact. 2003. p. 1–35.
[66] Pryor S, Barthelmie R. Assessing climate change impacts on the near-term stability of the wind energy resource over the United States. Proc Natl Acad Sci Unit States Am 2011;108(20):8167–71.